Survey of the class of isovalent antiperovskite alkaline earth-pnictide compounds

Wen Fong Goh and Warren E. Pickett
Department of Physics, University of California, Davis CA 95616, USA

(Dated: October 7, 2017)

The few reported members of the antiperovskite structure class $Ae_3Pn_APn_B$ of alkaline earth (Ae = Ca,Sr,Ba) pnictides (Pn = N,P,As,Sb,Bi) compounds are all based on the B-site anion Pn_B=N. All fit can be categorized as narrow gap semiconductors, making them of interest for several reasons. Because chemical reasoning suggests that more members of this class may be stable, we provide here a density functional theory (DFT) based survey of this entire class of $3 \times 5 \times 5$ compounds. We determine first the relative energetic stability of the distribution of pairs of Pn ions in the A and B sites of the structure, finding that the B site always favors the small pnictogen anion. The trends of the calculated energy gaps with Ae cation and Pn anions are determined, and we study effects of spin-orbit coupling as well as two types of gap corrections to the conventional DFT electronic spectrum. Because there have been suggestions that this class harbors topological insulating phases, we have given this possibility attention and found that energy gap corrections indicate the cubic structures will provide at most a few topological insulators. Structural instability is addressed by calculating phonon dispersion curves for a few compounds, with one outcome being that distorted structures should be investigated further for thermoelectric and topological character. Examples of the interplay between spin-orbit coupling and strain on the topological nature are provided. A case study of Ca_3BiP including the effect of strain illustrates how a topological semimetal can be transformed into topological insulator and Dirac semimetal.

PACS numbers:

I. INTRODUCTION

Oxide-based perovskites are the most studied class of ternary compounds for several reasons. First, oxygen is abundant and a great deal is known about oxide chemistry. Second, the basic cubic structure ABO_3 is simple and is governed to a great extent by ionic bonding. Third, given the near universal valence state O^{-2}, the A and B cation valences must total six, leaving a large number of combinations 1:5, 2:4, 3:3, 4:2, 5:1, considering the number of atoms that can assume these formal valences. Most importantly perhaps is the vast range of properties displayed by oxide perovskites, including high temperature superconductivity, much unusual magnetism, charge, spin, and orbital ordered phases, large linear responses (viz. Born effective charges that can differ by a factor of two or more from the formal charge), multiferroic states, among others.

Halide-based perovskites, viz. $KMnF_3$ with a monovalent anion, are a closely related class of materials. They are much less prevalent because only 1:2 and 2:1 cation charge pairs are possible, and the higher eletronegativity makes synthesis less straightforward. Less common still are nitrogen based perovskites, because the N^{-3} ion requires cations with formal charge pairs 4:5 or 3:6; higher formal valences are rare. N-based perovskites have been the topic of a high-throughout computational study to determine stable examples.[1]

Within a given crystal structure it is uncommon, but possible, to interchange the anion and cation sites. The *antiperovskite* class discussed here will be denoted Ae_3AB, where A is the (alkaline earth) cation on the oxygen site and A and B are anions that provide charge balance. Anion formal valences are practically limited to 1, 2, and 3, constraining considerably the cation valences. In this paper we will focus on divalent alkaline earth cations, for which the anion formal charges must sum to six, so it can be expected that nearly all of such antiperovskite compounds will have two trivalent anions. Here we consider the class in which both A and B anions are from the pnictogen column of the period table. Given the formal charge balance between divalent cations and trivalent anions, this class can be anticipated to harbor insulators and perhaps semimetals. Sun and coauthors have proposed that topological insulating phases may arise in the Ae_3BiN group with application of uniaxial strain,[2] providing additional current interest.

Examples of alkaline earth-pnictide antiperovskite compounds have been reported. Some crystallize in cubic structure,[3] while others show structural distortions[4] or even form distinct structures, *e.g.* the two compounds Ba_3(Sb,Bi)N assume the hexagonal antiperovskite structure[5], suggested to be due to the presence of large radii alkaline earth ions. The electronic state of this class of materials is insulating, ranging from relatively wide gap insulating to narrow gap semiconducting. The reported compounds will be discussed in Sec. III D in relation to our results. Notably, compounds in this class with pnictides other than N inside the octahedron have not been reported.

Density functional theory (DFT) based study of insulating $BiNCa_3$ and metallic $PbNCa_3$ provided the underlying electronic structure (as shown in the current paper) of this class of materials.[6] DFT based results for the band structure and pressure dependence of the gap have been reported for several of these compounds, discussed in Sec. IIID below. Motivated by the relatively few known examples and the broad possibilities for new

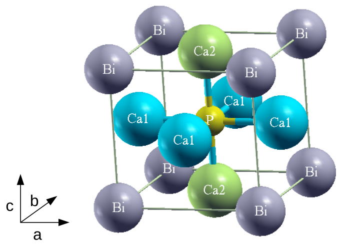

(a) Tetragonal crystal structure of strained Ca_3BiP.

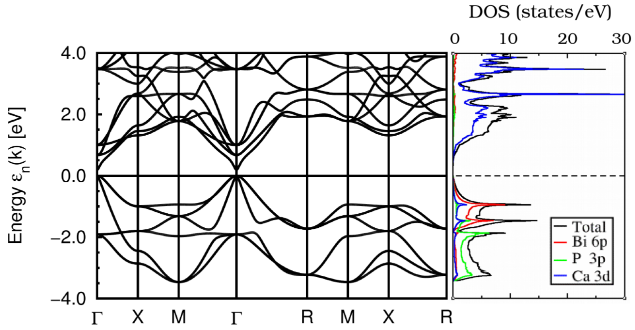

(b) Band structure and density of states of cubic Ca_3BiP.

FIG. 1: (a) The antiperovskite structure of Ca_3BiP with tetragonal compression along (001), the space group becomes $P4/mmm$. Ca^{2+} ions lie on two nonequivalent sites(blue and green). (b) Band structure and density of states of cubic Ca_3BiP, without SOC. P $3p$ bands provide the lowest valence states, while Bi $6p$ bands comprise the highest valence states. Ca $4s$ and $3d$ orbitals dominate the lower conduction states. The gap of 0.2 eV occurs at Γ, throughout the rest of the zone the gap is large.

materials with important properties, we have carried out a survey on the entire class of $3 \times 5 \times 5$ alkaline earth-pnictide antiperovskite compounds, viz. $Ae_3Pn_APn_B$, where $Ae = \mathrm{Ca, Sr, Ba}$ and $Pn_A, Pn_B = \mathrm{N, P, As, Sb, Bi}$, using first principles DFT methods. The conventional ordering of atoms Pn_A and Pn_B will follow that of a perovskite with general chemical formula ABO_3, where the A cation is 12-fold cub-octahedral coordinated and B is 6-fold coordinated by an octahedron of O anions. In the case of antiperovskite $Ae_3Pn_APn_B$, Pn_B is inside the Ae_6 octahedron while Pn_A sits in the more open A site.

The manuscript is organized as follows. The computational methods are summarized is Sec. II. Section III contains much of the basic results, and includes a general analysis of the common features of these antiperovskites, the correction to DFT bandgaps that are important for small (or negative) gap compounds, and a synopsis of previously reported or predicted members of this class. The possibility of topological character, and the favorable candidates, are described Sec. IV. Section V addresses the question of structural stability with two examples, and a concise summary is given in Sec. VI.

II. COMPUTATIONAL METHODS

To study the electronic structure of these 75 compounds, the generalized gradient approximation (GGA) exchange-correlation functional of Perdew-Burke-Ernzerhof-1996[8] was used, as implemented in the full-potential local orbital (FPLO)[9] scheme. Self-consistency was obtained on a dense k-mesh of $20 \times 20 \times 20$ to ensure good convergence of the density and thereby the eigenvalues. The fully relativistic Dirac four component equations implemented in FPLO were performed to include spin-orbit coupling and other relativistic corrections. The cubic lattice constants were obtained by minimizing the energy with respect to volume.

In small gap compounds, and especially for potential topological materials where gaps are typically quite small, the underestimate of the band gap by the GGA functional must be dealt with. We have calculated band gap corrections of the $Ae_3\mathrm{Bi}Pn_B$ subclass using the modified Becke-Johnson (mBJ) exchange-correlation potential. This scheme provides a self-energy-like correction to eigenvalues that has been found to be realistic for several semiconductors and insulators.[10,12,13] A formally well justified means of obtaining self-energy corrections is provided by GW approximation.[11,14] We have used the FHI-gap implementation[11] in the WIEN2K code[15] on four compounds, and make comparison with the mBJ results in Sec. III. In this $G_\circ W_\circ$ implementation the eigenvalue in $G_\circ$ is iterated to self-consistency. The linearized augmented plane wave basis was specified by R_mG_{max}=7, where R_m in the minimum radius of the atomic spheres and G_{max} is the largest reciprocal lattice vector. For the $G_\circ W_\circ$ version of GW implemented in FHI-gap, the mixed basis quality was determined by $\ell_{max} = 3$, $Q = 0.75$. Unoccupied states up to 1000 eV were summed over, the number of discrete imaginary frequency points was 16, and the k-point mesh was $3 \times 3 \times 3$. Increasing the latter to $4 \times 4 \times 4$ resulted in self-energy changes of the order of 0.01 eV.

III. ANALYSIS OF CUBIC STRUCTURES AND SPIN-ORBIT COUPLING

A. Cell volume and energetic stability

The cubic antiperovskite $\mathrm{Ae_3Pn_APn_B}$ structure[5] (space group $Pm\bar{3}m$) has an Ae_6Pn_B octahedron, with Pn_A surrounded symmetrically by eight octahedra, with the primitive cell pictured in Fig. 1a. For the cubic (undistorted) structure, the equilibrium lattice constant has been obtained for all $3 \times 5 \times 5$ combinations. These results and the following data are presented in Table I. First is a comparison of the energy difference upon interchange $Pn_A \leftrightarrow Pn_B$ of the two Pn ions. It is always the case that it is energetically favorable to have the smaller Pn ion in the Pn_B octahedron position. Energy differences, which range from 0.2-4.3 eV, are largest when N

TABLE I: Data on the complete class of $Ae_3Pn_APn_B$ antiperovskites. a(Å) gives the optimized lattice constants in Å. $\Delta E = E_{Ae_3Pn_APn_B} - E_{Ae_3Pn_BPn_A}$ provides the energy difference in eV. Since this energy difference is antisymmetric across the diagonal, the energy differences are only shown in the lower left triangle for the stable phase (the smaller Pn ion is always Pn_B). ε_g and ε_g^{SOC} give the band gap (without and with SOC) in eV; of either a small positive or negative (negative indirect band gap) value, with an exception of a few with bands crossing at the Fermi level or gapless states (represented by SM for semimetallic or M for metallic state). Only the ν_0 Z_2 index is provided, because all $\nu_{1,2,3}$ are zero. Values in bold indicate a topological semimetal state.

		N_B					P_B					As_B					Sb_B					Bi_B				
		a(Å)	ΔE(eV)	ε_g(eV)	ε_g^{SOC}(eV)	Z_2	a(Å)	ΔE(eV)	ε_g(eV)	ε_g^{SOC}(eV)	Z_2	a(Å)	ΔE(eV)	ε_g(eV)	ε_g^{SOC}(eV)	Z_2	a(Å)	ΔE(eV)	ε_g(eV)	ε_g^{SOC}(eV)	Z_2	a(Å)	ΔE(eV)	ε_g(eV)	ε_g^{SOC}(eV)	Z_2
N_A	Ca	4.61	-	0.	0.	1	5.29	-	SM	M	1	5.42	-	0.	0.	1	5.76	-	-0.01	-0.02	1	5.85	-	-0.01	-0.04	1
	Sr	4.99	-	0.	0.	1	5.67	-	0.	0.	1	5.80	-	0.	-0.01	1	6.13	-	-0.02	-0.03	1	6.23	-	-0.02	-0.05	1
	Ba	5.33	-	SM	SM	1	6.03	-	-0.04	-0.05	1	6.18	-	-0.05	-0.06	1	6.52	-	-0.07	-0.08	1	6.61	-	-0.05	-0.12	1
P_A	Ca	4.73	-2.96	0.85	0.85	0	5.31	-	0.33	0.31	0	5.42	-	0.10	0.05	0	5.74	-	0.	0.	1	5.82	-	0.	0.	1
	Sr	5.09	-2.55	0.45	0.45	0	5.67	-	0.	0.	1	5.79	-	0.	0.	1	6.09	-	0.	0.	1	6.17	-	0.	0.	1
	Ba	5.43	-2.28	SM	SM	0	6.02	-	0.03	0.01	1	6.14	-	0.	0.	1	6.44	-	0.	0.	1	6.53	-	0.	-0.10	1
As_A	Ca	4.78	-3.38	0.77	0.72	0	5.34	-0.55	0.15	0.09	0	5.45	-	0.	0.	1	5.75	-	0.	0.	1	5.84	-	0.	0.	1
	Sr	5.13	-2.93	0.30	0.28	0	5.70	-0.50	0.	0.	**1**	5.81	-	0.	0.	1	6.11	-	0.	0.	1	6.19	-	0.	-0.01	1
	Ba	5.47	-2.64	SM	SM	0	6.04	-0.46	0.	0.	**1**	6.16	-	0.	0.	1	6.46	-	0.	-0.02	1	6.54	-	0.	-0.14	1
Sb_A	Ca	4.88	-4.26	0.46	0.35	0	5.39	-1.76	0.65	0.50	0	5.49	-1.2	0.40	0.22	0	5.78	-	0.07	0.	1	5.86	-	0.	0.	1
	Sr	5.22	-3.77	0.20	0.15	0	5.74	-1.58	0.30	0.16	0	5.84	-1.08	0.10	0.	**1**	6.13	-	0.	0.	1	6.21	-	0.	0.	1
	Ba	5.55	-3.40	SM	SM	0	6.08	-1.45	0.28	0.18	0	6.19	-0.99	0.13	0	**1**	6.48	-	0.	0.	1	6.55	-	0.	-0.12	1
Bi_A	Ca	4.92	-4.35	0.48	0.07	0	5.42	-1.99	0.16	0.	**1**	5.53	-1.44	0.	-0.03	**1**	5.81	-0.29	0.	-0.10	**1**	5.89	-	0.	-0.12	0
	Sr	5.26	-3.86	0.25	0.01	0	5.77	-1.75	0.	-0.02	**1**	5.88	-1.26	0.	-0.05	**1**	6.15	-0.20	0.	-0.10	**1**	6.23	-	0.	-0.13	0
	Ba	5.59	-3.47	SM	SM	0	6.11	-1.61	0.	-0.05	**1**	6.22	-1.17	0.	-0.10	**1**	6.50	-0.21	0.	-0.18	**1**	6.58	-	0.	-0.17	0

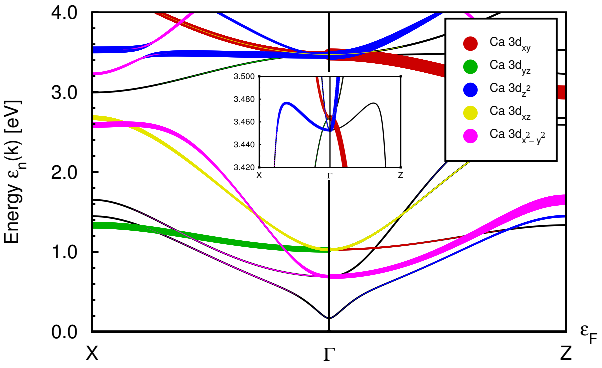

FIG. 2: Color plot differentiating orbital character, showing the band ordering of $3d$ orbital energies of the apical Ca ions located at $(\frac{1}{2}, \frac{1}{2}, 0)a$ in the unit cell. The insert provides an enlargement of the complex near Γ around 3.5 eV, showing that the d_{xy} and d_{z^2} levels are nearly degenerate at Γ.

is one of the ions, and the magnitude of the difference increases with difference in atomic number of the anions. These trends can be understood from Coulomb energetics: if the smaller anion is surrounded by the cation octahedron, the attractive Coulomb energy will be larger. An additional factor is that the A site naturally accommodates a bigger atom than will the B site, giving better volume filling by atoms. The other data in Table I will be discussed below.

B. Electronic band structure

For general orientation, the electronic structure and DOS of a representative compound, Ca_3BiP containing the largest and the next to smallest pnictide ions, is shown in Fig. 1b. A generic feature in this class of perovskites is that the smaller Pn_B p bands lie lower than the Pn_A p bands, making the larger ion (which conveniently also has the largest SOC) the one of interest in determining the band gap (or not) and subsequently the topological character. Since both A and B sites have cubic symmetry, both Pn p band complexes have threefold degeneracy at the Γ point when SOC is neglected, and SOC separates the eigenvalues into $p_{1/2}$ and $p_{3/2}$ states, with the latter for Pn_B forming the top of the valence bands.

In the conduction bands three sets of five Ae d bands dominate. Unexpectedly, a "free electron like" band that has no single dominant orbital character, discussed below, lies near the bottom of the conduction bands at Γ and often is the band at the conduction band minimum. Since the Ae site has tetragonal symmetry, the d shell is split by the crystal field into a d_{xz}, d_{yz} doublet and three singlets $d_{xy}, d_{x^2-y^2}, d_{z^2}$, relative to the local (z) axis. For some purposes it would be important to consider how these thirty orbitals on six Ae ions form molecular orbitals on the Pn_BAe_6 octahedron. Actually performing and applying such a transformation is complicated by the fact that each Ae ions' orbitals are shared with two octahedra.

One fundamental interaction at and near Γ is that of the Pn_A p states with the d orbitals of the twelve Ae ions coordinating it, and with the diffuse "s" band. To assist understanding of the ordering of the Ae d characters at the Γ point, the orbital characters in the d band region of the apical Ca ion (whose local axis is along the $\hat{z}$ direction) are plotted in Fig. 2. Ca d_{xy} and d_{z^2} have orbital density oriented towards four nearest Bi^{-3} ions and two nearest P^{-3} ions respectively, and their orbital energies are close and are higher than for the other d orbitals. The $d_{x^2-y^2}$ orbital lies lowest in energy, corresponding to an orbital density directed between negative ions, being lower than the highest d orbital by 2.8 eV. This separation changes to 3.6 eV and 3.3 eV by replacing Ca with

Sr and Ba respectively. The degenerate d_{xz}, d_{yz} orbitals lie about 0.4 eV above the $d_{x^2-y^2}$ orbital. The Pn_A p bands approach and mix with the Ae d bands around the Γ point, with a substantial band gap throughout the rest of the zone.

Trends in band gaps. We here review the behavior of the gaps of the more stable members, which lie in the lower left triangle of Table I. We consider the bands without SOC, which are simpler from which to derive chemical trends. For N_B (N on the B site), the Ca compounds have gaps that decrease from 0.85 eV to 0.48 eV for the progression from P_A to Bi_A. The corresponding Sr compounds have smaller gaps, 0.45 eV to 0.25 eV, and for the Ba compounds there is band overlap (negative overlap). Moving to P_B and on to Bi_B, there is no monotonic progression of gaps, but a clear trend to smaller or zero gaps at the B site atom becomes heavier. Evidently SOC, which splits the valence band maximum, will decrease the gap size and in some cases lead to gap inversion (reported in the table as zero gap or negative indirect gap).

Topological character. One of the motivations of this survey of 75 compounds was to begin to assess the likelihood of finding topological insulating, or also topological semimetal, phases in these antiperovskites. We return to this topic in Sec. IV. However, in Table I we have provided the Z_2 topological index for the compounds and structures we have studied, for the GGA+SOC bands. In the lower left subdiagonal of Table I that contains the more stable ordering of the Pn_A, Pn_B pairs, we find no topological bands in the N_B column. However, moving to the heavier Pn_B columns, many $Z_2 = 1$ results are obtained. The profusion of these values appear at first sight to promote optimism. There are important caveats, however. First, GGA calculations are known to underestimate bandgaps in insulators. Self-energy corrections to the gap are discussed in Sec. IIIC. Secondly, stability of these model compounds is an issue. Only a few have been reported, which we discuss in Sec. III D. Some may be thermodynamically unstable with respect to more stable phases, while other may be dynamically unstable and distort to a lower symmetry structure with an altered electronic structure. We return to the question of topological character in Sec. IV.

C. Energy Gap Correction

We define the inversion energy as the energy of the conduction band minimum minus the energy of the valence band maximum (which is that of the A site p-band). (In the case the B site atom is N, the VBM is a strong admixture of Pn_A and N p character.) A negative inversion energy indicates the band inversion that is essential for topological character. Table II provides the inversion energy and band gap for GGA+SOC eigenvalues, with and without mBJ. Note that the band gap, once SOC is included, usually appears away from the Γ point, thus is not equal to the inversion energy. The effect of including mBJ is a separation of conduction bands from valence bands (inversion energy) of 1.0, 0.7, 0.7, 0.6 eV for N, P, As, Sb, respectively, a very systematic trend independent of the cation Ca, Sr, Ba. The final (GGA+mBJ+SOC) band gap, if nonzero, is less regular because it occurs away from the Γ point and is more dependent of details of the dispersion and inversion energy.

Only the Ae_3BiSb compounds show negative inversion energy when the mBJ correction is included. Sr_3BiAs has very small positive inversion energy (0.06 eV). The rest are normal insulators. Many of these inversion energies, positive or negative, are small enough that they can be manipulated by pressure or strain, with an example discussed in Sec. IV.

The bands of the four compounds we have chosen are shown in Fig. 3, all being based on Bi on the A site to provide the largest effect of SOC. Ca_3BiN in Fig 3(a) provides the reference normal insulator situation, with a two-fold level (A atom $p_{3/2}$) at the VBM and a doublet and a somewhat higher singlet in the lower conduction bands. The bands for the three cases, GGA(SOC), GGA(SOC)+mBJ, GGA(SOC)+$G_\circ W_\circ$, are aligned at the valence band maximum (VBM). The corrections to the valence bands are not very important for our current considerations, but the two corrections are rather small but not necessarily similar. The conduction band corrections are larger in the region pictured, about 0.5 eV, and similar in the low energy region that is shown. Comparison between mBJ and GW corrections have been commented on previously.[17]

Figure 3(c) shows the Sr analog, Sr_3BiN. Its gap is smaller, but more interesting is that the conduction band singlet has dropped close to the doublet. Unexpectedly, the $G_\circ W_\circ$ correction has dropped to 0.15 eV while mBJ remains near 0.5 eV. The corrections in the valence bands remain small, and again the two corrections are not always similar.

Band inversion occurs for Ca_3BiP shown in Fig. 3(b), due to the conduction band singlet dropping not only below the doublet, but also below the VBM doublet. One crucial result is that the band structure becomes that of a zero-gap semiconductor. Away from Γ the bands hybridize, complicating the process of following the underlying bands. However, the inversion becomes clear when it is noticed that both self-energy corrections *raise* the Γ GGA(SOC) eigenvalue at -0.3 eV, consistent with conduction eigenvalue character, which is also confirmed by its positive parity eigenvalue.

This behavior is repeated for Sr_3BiAs shown in Fig. 3(d), where the band orderings and corrections are somewhat different than in Ca_3BiP and may be easier to follow. Even in GGA(SOC) the low energy band structure can be quite delicate, but becomes more so in the presence of self-energy corrections. This complex behavior will be explored on more detail elsewhere.

and $Pn = \mathrm{N, P, As, Sb, Bi}$ with SOC and mBJ correction.

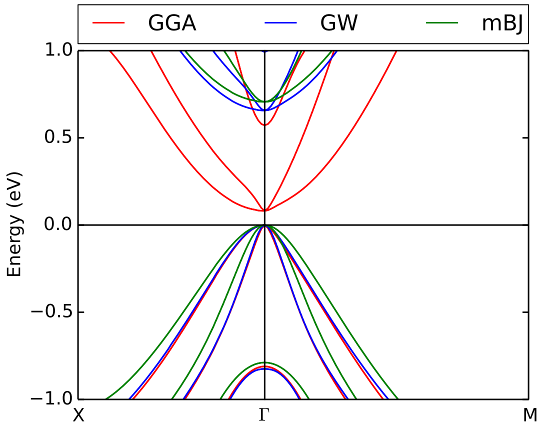

(a) Ca_3BiN

(b) Ca_3BiP

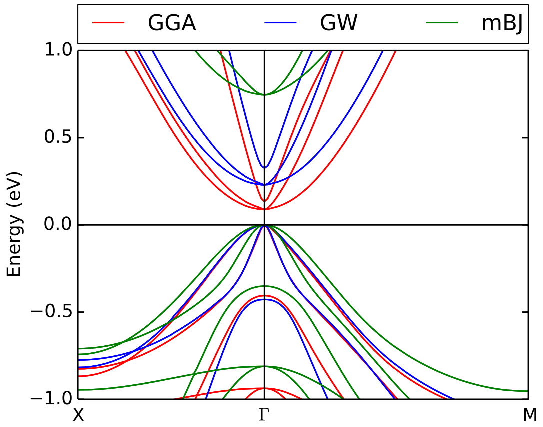

(c) Sr_3BiN

(d) Sr_3BiAs

FIG. 3: GGA (red), $G_\circ W_\circ$ (blue) and mBJ (green) energy bands along X - Γ - M directions, for four antiperovskite compounds. All include spin-orbit coupling.

TABLE II: Inversion energy and band gap of $Ae_3\mathrm{Bi}Pn$, where Ae = Ca, Sr, Ba and Pn = N, P, As, Sb, Bi with SOC and mBJ correction. The mBJ effect is defined as the difference between with and without mBJ.

$Ae_3\mathrm{Bi}Pn$	Pn	N			P			As			Sb		
Ae		SOC	SOC + mBJ	mBJ effect	SOC	SOC + mBJ	mBJ effect	SOC	SOC + mBJ	mBJ effect	SOC	SOC + mBJ	mBJ effect
Ca	Inversion Energy	0.572	1.587	1.015	-0.283	0.460	0.743	-0.533	0.188	0.721	-0.754	-0.149	0.604
	Band Gap	0.081	0.706	0.625	0	0.460	0.460	0	0.188	0.188	0	0	0
Sr	Inversion Energy	0.133	1.138	1.005	-0.458	0.286	0.744	-0.658	0.063	0.721	-0.831	-0.226	0.605
	Band Gap	0.088	0.746	0.658	0	0.286	0.286	0	0.063	0.063	0	0	0
Ba	Inversion Energy	0.003	1.010	1.007	-0.264	0.464	0.727	-0.427	0.283	0.709	-0.633	-0.034	0.599
	Band Gap	0	0.483	0.483	0	0.464	0.464	0	0.283	0.283	0	0	0

D. Reported antiperovskites

Relatively few of this class of antiperovskite compounds have been synthesized, often without full characterization, and only nitrides. Most of these are based on the Ca^{2+} cation. All four of Ca_3Pn_AN were reported to be either semiconducting (Pn_A=Bi,Sb) or insulating (Pn_A=As,P).[3] Our calculated band gaps from Table I also indicate semiconducting states, as did previous work on some of these members[18] and the Sr and Ba counterparts $(Sr,Ba)_3(Sb,Bi)N$.[19] When Bi is substituted by the smaller pnictides Sb, As, and P, the band gap increases, because as the electronegativity decreases, the energy level of the p anion relative to the cation level decreases as well.

Structurally, the Pn_A=Bi and Sb members of Ca_3Pn_ABi are cubic, while (presumably) the size mismatch for the smaller ions Pn_A=As and P anions led to orthorhombic $Pnma$ distortion.[4] Niewa's review reported $Sr_3(Sb,Bi)N$ as cubic, as well as $Mg_3(As,Sb)N$[20] which are not included in our study.[5] In contrast, a hexagonal structure was reported for $Ba_3(Sb,Bi)N$, built on

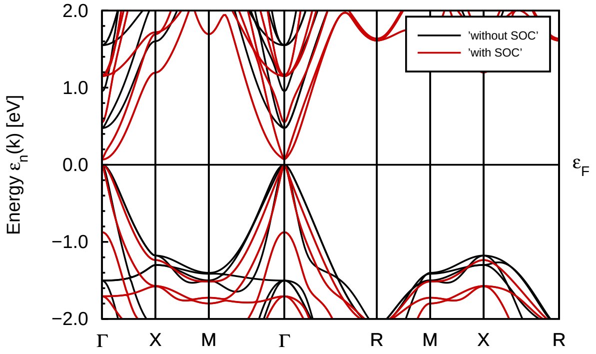

(a) Ca_3BiN, a normal insulator with small gap.

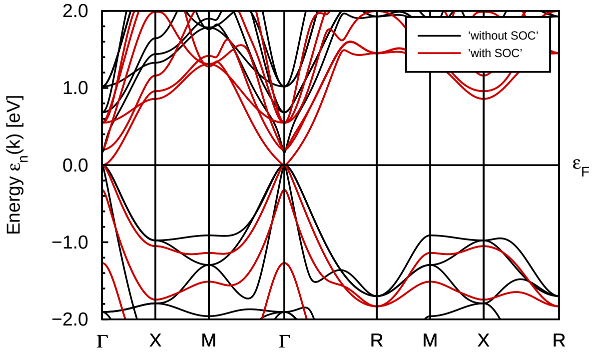

(b) Ca_3BiP, a topological semimetal with CBM and VBM touching.

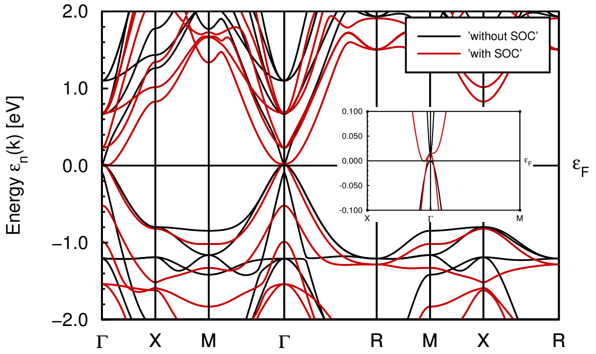

(c) Sr_3BiP, a topological semimetal with delicate hole pockets, as indicated in the inset.

FIG. 4: The $Ae_3Pn_APn_B$ antiperovskite compounds can be classified into three categories based on their electronic structure and topological invariants. The electronic band structures of Ca_3BiN, Ca_3BiP and Sr_3BiN, from top to bottom, are used as examples of each category.

face-sharing rather than corner-linked octahedra. Such a hexagonal structure tends to be favored by compounds containing alkaline-earth metal species with large radii. Coulomb repulsion between N in face-sharing octahedra and the resulting distance d(N-N) has been suggested to play a role in stabilizing the structure.[5,19] d(N-N) for Ba_3(Sb,Bi)N is 3.30Å, which is sufficiently large to stabilize the hexagonal structure.

Some of these small gap compounds have been calculated to be promising thermoelectric materials[7,18] with high thermodynamic figure of merit. viz. Sr_3(Sb,Bi)N.[7] The pair Magnetic susceptibility and electrical resistivity data indicate that the compounds are diamagnetic semiconductors. The optical band gaps of Sr_3SbN and Sr_3BiN are reported to be 1.15 eV and 0.89 eV, respectively.[19]

First-principle calculations have been reported for some of the mentioned compounds, largely to assess specific properties such as their elastic behavior and optical response.[21–31] Our survey should be useful in interpretation of those results, by connecting their computed properties to similarities and differences in their electronic structures.

IV. ON THE POSSIBILITY OF TOPOLOGICAL CHARACTER

The Z_2 invariant ν_0 determines the topological nature of an insulator, and for inversion symmetric crystals the parity criteria proposed by Fu and Kane[32] determines the topological character. Specifically, the sum of the parities δ_i at occupied states at the time-reversal invariant momenta (TRIM) determines the primary Z_2 invariant ν_0:

$$(-1)^{\nu_0} = \prod_{i=1}^{8} \delta_i \tag{1}$$

By studying Table I it can be found that the electronic structure and topological nature of these compounds can be classified into three categories: (i) small gap with a topologically trivial phase, viz. Ca_3BiN in Fig. 4a, (ii) the VBM and conduction band minimum (CBM) touch at Γ point with Z_2 indices of (1;000), as for Ca_3BiP in Fig. 4b), and (iii) there are (usually tiny) electron and hole pockets along high symmetry lines with Z_2 indices of (1;000) as in the example of Sr_3BiP in Fig. 4c).

For the first type, band inversion is not present for the cubic structure but the application of strain may lead to inversion and a topological material.[2] For the second and third types (highlighted in bold in Table I), the band inversion is induced by SOC of the heavy elements.[33] No gap is opened, however, leaving these systems as topological semimetals. Strain can be used to induce a transition from topological semimetal to topological insulator, provided that the band overlapping (especially for type (iii)) is not greater than the effect of SOC.

A case study of Ca_3BiP will be used to demonstrate the role that interplay of SOC and strain play in band inversion of the second and third class above. Figure 5 shows the schematic energy level diagram of Ca_3BiP at the Γ point, along with the bands around Γ for the same conditions. Cubic Ca_3BiP has an energy gap of 0.2 eV. At the Γ point, the valence bands comprised of Bi $6p$ characters and P $3p$ characters have negative parities, while the s character of the conduction band minimum has positive parity. (There are substantial gaps at all other TRIMs, so their contributions to Z_2 are invariant to all changes and are the same for all of these antiperovskite compounds.) The strong SOC of Bi inverts the s conduction band and the valence Bi $6p$ bands. No gap is opened, however, resulting in a topological semimetal phase.

With a tetragonal compression of 5% along (001), the degeneracy is lifted and a small gap of 34 meV is produced while maintaining the inverted band ordering. The strain does not violate inversion symmetry, but merely splits the degeneracy of the Γ_8^- band at the Fermi level into two sets of Kramer doublets, with odd parity below the Fermi level and even parity above, so the parity eigenvalues are unchanged. This mechanism is similar to that of $\alpha-$Sn and HgTe topological insulators.[32,34] Although HgTe does not have inversion symmetry, it can be argued that this compound in group II-VI can be treated as adding a inversion symmetry breaking perturbation into group IV element, like Tin in the α or gray phase.

The transition from the topological semimetal state to a topological insulator can also be realized by compressing the lattice parameter c by a few percent, which can be accomplished by growth of thin films on a substrate with the corresponding lattice parameter.. As shown in Fig. 6, a small energy band gap with SOC is produced within this range, with a maximum gap of 40 meV occurring at 3% compression. The band parity remain odd within this range, but goes back to even at 8% compression. On the other hand, uniaxial expansion along the c-axis opens up a gap except along k_z, where a Dirac-like band crossing occurs, producing a topological Dirac semimetal (Fig. 5(f)). However, not all direction of strain application will open up a gap. For example, applying uniaxial strain along (111) direction does not open up a gap, because the Bi p_x, p_y and p_z characters still remain equivalent.

V. STRUCTURAL (IN)STABILITY

The oxide perovskite structure is notoriously subject to distortion from the ideal cubic structure, for two primary reasons. First, perovskite is not a close-packed structure. Especially the BO_2 (001) layer (viz. the CuO_2 layer in high temperature superconducting cuprates) is not: atoms are aligned in rows with an empty site of square symmetry. Second, there is tension between the preferred lattice constants of the BO_2 layer and the AO layer. The mismatch is quantified by Goldschmidt's ratio, using established ionic radii and quantifying the mismatch as a percentage. It may be expected that these antiperovskites being studied may be subject to similar issues. Unfortunately, these antiperovskites comprise a new class of compounds for which appropriate ionic radii have not been established.

Calculation of the phonon spectrum is commonly used to assess dynamical stability of a compound. Antiperovskites with N atom at the B-site have been studied both experimentally and computationally[4,5,7,18,19,21–31]. However, B-site cations other than N have not yet been incorporated into this structure. We have calculated the phonon dispersion curves for Ca_3BiN and for Ca_3BiP to assess their stability. The results are presented in Fig. 7.

For Ca_3BiN, all frequencies are positive and the Bi atom dominates the acoustic frequencies up to 75 cm^{-1}. Ca atoms dominate frequencies in the $100-300$ cm^{-1} range, while the light N atom oscillates in the highest frequency 400-475 cm^{-1} region. The phonon spectrum of Ca_3BiP is quite different. The overriding feature is the imaginary frequencies around both the M and R points of the zone. The atomic displacements at these points give insight into the structural instability; the unstable modes have Bi+Ca character. At the M point, the Bi and P atoms are fixed while the Ca atoms rotate around the principal axis, thus the crystal is unstable to such rotations. Allowing the octahedron to rotate around z-axis as shown in Fig. 8, the energy is lowered by 0.2 eV. The electronic rearrangement due to this distortion leaves Ca_3BiP as a conventional insulator.

Distortion of antiperovskites compounds with heavier Pn_B elements, viz. Ae_3BiSb with Ae=Ca, Sr, and Ba, were studied as well. Distortions from cubic structure were favored by $0.7-0.8$ eV per formula unit. The resulting band structures are those of a Dirac semimetal, hosting Dirac points along the $\Gamma-Z$ direction as shown for Ca_3BiSb in Fig. 9. However, applying the mBJ correction widens that gap to around 0.4 eV and leaves them in conventional insulator states.

VI. SUMMARY

The stability, electronic structure and topological aspect of the class of isovalent antiperovskite alkaline earth-pnictide compounds have been studied using DFT. This class with pnictide other than N inside the octahedron is distorted with the octahedron rotated along a principal axis. The electronic structures of these compounds with SOC can be classified into three categories. First, one common class of the topological aspect is that the electronic structure is gapped with a topologically trivial phase. Second, a zero gap semiconductor with VBM and CBM touching at Γ point with a Z_2 invariant of 1;000. Third, a semimetal consists of electron or hole pockets of maximum 0.1 eV energy and band degenerate at Γ point with a Z_2 index of 1;000. Strain is required to produce a topological insulator. While the first type (e.g. Ca_3BiN^2) needs both SOC and proper strain to have band order-

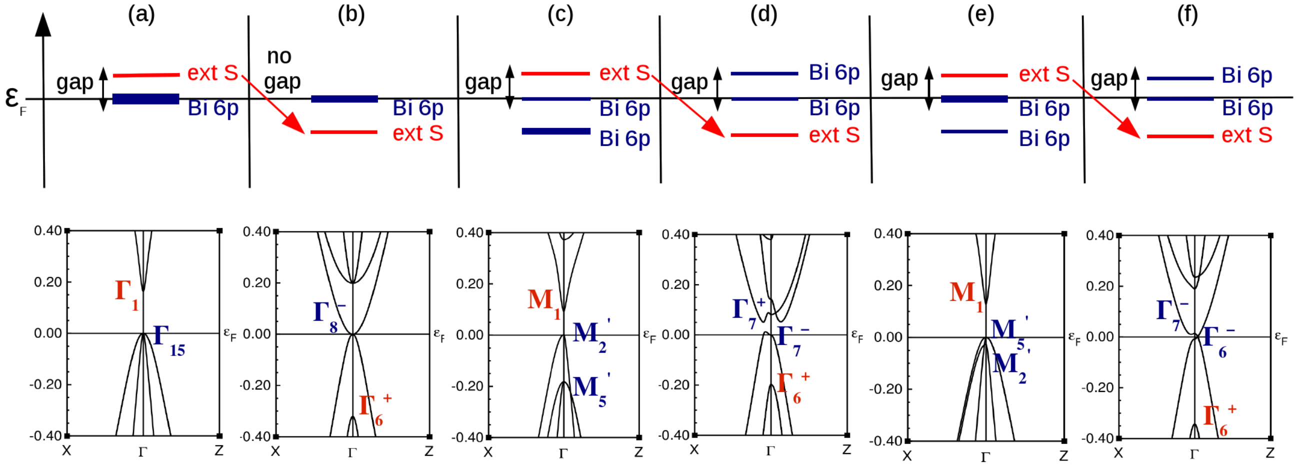

FIG. 5: Upper panel: Schematic energy diagram of Ca_3BiP at Γ point (a) without SOC, (b) with SOC, (c) with compressive strain and without SOC, (d) with 5% compressive strain and SOC, (e) with 1% expansive strain and without SOC and (f) with expansive strain and SOC. Ultra-fine, fine and thick lines represent 1-fold, 2-fold and 3-fold degeneracy (not including spin degeneracy) respectively. Lower panel: Band structures along X − Γ − Z with irreducible representations given (in Bouckaert-Smoluchowski-Wigner notation) at the Γ point.

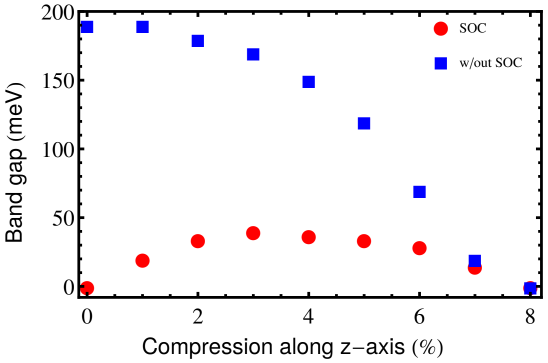

FIG. 6: Band gap of Ca_3BiP versus compression, showing the effect of SOC. Compression of along (001) without SOC closes the band gap. When SOC is included the band gap is closed, but then is re-opened by strain.

ing inverted, the second and third types (e.g. Ca_3BiP and Sr_3BiP) only need SOC to induce the band inversion, giving a Z_2 invariant of 1;000, but in a topological semimetal state, whereupon compressive strain may produce a transition to topological insulator. On the other hand, expansive strain may give rise to Dirac semimetals. With proper strain engineering, some may become a promising topological insulator and Dirac semimetal, as witness in Ca_3BiP and Sr_3AsP antiperovskite compounds.

VII. ACKNOWLEDGMENTS

We acknowledge useful comments from Theo Siegrist and Mas Subramanian about pnictide-based antiperovskite and nitride perovskite synthesis. This work was supported by the NSF DMREF program through grant DMR-1534719. Computational data for the compounds in Table I was uploaded to the DOE-supported Materials Project.

---

[1] R. Sarmiento-Pérez, T. F. T. Cerqueira, S. Körbel, S. Botti, and M. A. L. Marques, Prediction of Stable Nitride Perovskites, *Chem. Mater.* **27**, 5957 (2015).

[2] Y. Sun, X.Q. Chen, S. Yunoki, D. Li and Y. Li, New family of three-dimensional topological insulators with antiperovskite structure, *Phys. Rev. Lett.* **105**, 216406 (2010).

[3] M. Y. Chern, D. A. Vennos, F. J. DiSalvo, Synthesis, Structure, and Properties of Anti-perovskite Nitrides Ca_3MN, M= P, As, Sb, Bi, Ge, Sn, and Pb, *J. Solid State Chem.* **96**, 415 (1992).

[4] M. Y. Chern, F. J. DiSalvo, J. Parise, and J. A. Goldstone, The Structural Distortion of the Anti-perovskite Nitride Ca_3AsN, *J. Solid State Chem.* **96**, 426 (1992).

[5] R. Niewa, Alkaline-earth Metal Nitrides of the Main-Group Elements: Crystal Structures and Properties of Inverse Perovskites, *Z. f. anorg. allg. Chemie* **639**, 1699 (2013).

[6] D. A. Papaconstantopoulos and W. E. Pickett, Ternary nitrides $BiNCa_3$ and $PbNCa_3$: Unusual ionic bonding in the antiperovskite structure, *Phys. Rev. B* **45**, 4008 (1992).

[7] M. Bilal, Saifullah, M. Shafiq, B. Khan, H. A. R. Aliabad, S. J. Asadabadid, R. Ahmad, and I. Ahmad, Antiperovskite compounds $SbNSr_3$ and $BiNSr_3$: Potential

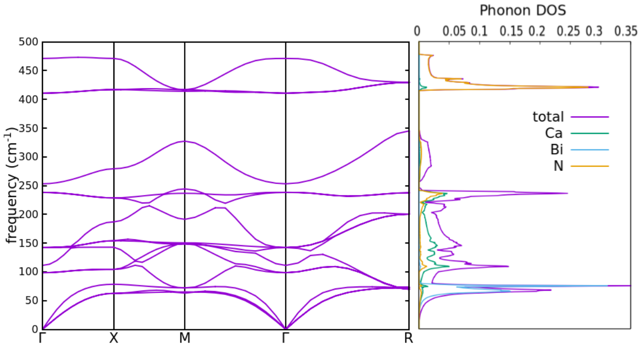

(a) Phonon modes of Ca_3BiN

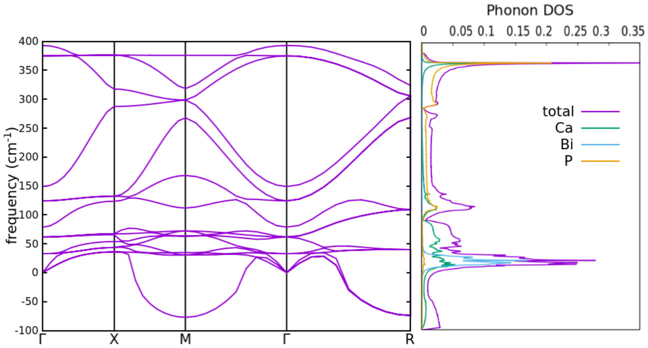

(b) Phonon modes of Ca_3BiP

FIG. 7: Calculated phonon dispersion of (a) Ca_3BiN and (b) Ca_3BiP. Imaginary frequencies (plotted as negative) indicate structural instability, which is severe for Ca_3BiP for both M and R point rotations.

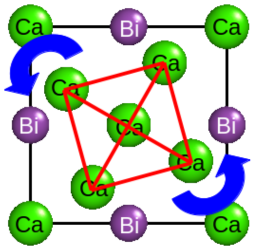

FIG. 8: Structure of distorted Ca_3BiP viewed along the z-axis, after the Ca octahedron (marked by red) has rotated around the z-axis.

candidates for thermoelectric renewable energy generators, *Phys. Lett. A* **379**, 2067 (2015).

[8] J.P. Perdew, K. Burke, and M. Ernzerhof, Generalized gradient approximation made simple, *Phys. Rev. Lett.* **77**, 3865 (1996).

[9] K. Koepernik and H. Eschrig, Full-potential nonorthogonal local-orbital minimum-basis band-structure scheme, *Phys. Rev. B* **59**, 1743 (1999).

[10] A.D. Becke and E.R. Johnson, A simple effective potential for exchange, *J. Chem. Phys.* **124** 221101 (2006).

[11] H. Jiang, R. I. Gomez-abal, X.-Z. Li, C. Meisenbichler, C. Ambrosch-Draxl, and M. Scheffler, FHI-gap: a *GW* code based on the all-electron augmented plane wave method, Comp. Phys. Commun. **184**, 348 (2013).

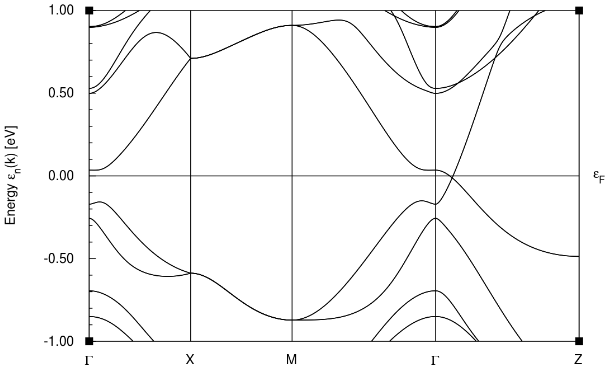

FIG. 9: Band structure of distorted Ca_3BiSb showing the Dirac point along $\Gamma - Z$ that pins the Fermi level.

[12] F. Tran, P. Blaha and K. Schwarz, Band gap calculations with Becke-Johnson exchange potential, *J. Phys.: Condens. Matter.* **19** 196208 (2007).

[13] F. Tran and P. Blaha, Accurate Band Gaps of Semiconductors and Insulators with a Semilocal Exchange-Correlation Potential, *Phys. Rev. Lett.* **102**, 226401 (2009).

[14] H. Jiang and P. Blaha, GW with linearized augmented plane waves extended by high-energy local orbitals, *Phys. Rev. B* **93**, 115203 (2016).

[15] P. Blaha, K. Schwarz, G.K.H. Madsen, D. Kvasnicka, and J. Luitz, *WIEN2K, An Augmented Plane Wave + Local Orbitals Program for Calculating Crystal Properties*, Karlheinz Schwarz, Techn. Universität Wien, Austria, 2001.

[16] T. Kariyado and M. Ogata, Low-energy effective hamiltonian and the surface states of Ca_3PbO, *J. Phys. Soc. Jpn.* **81**, 064701 (2012).

[17] J.A. Camargo-Martnez and R. Baquero, Performance of the modified Becke-Johnson potential for semiconductors, *Phys. Rev. B* **86**, 195106 (2012).

[18] M. Bilal, S. Jalali-Asadabadi, R. Ahmad, and I. Ahmad, Electronic Properties of Antiperovskite Materials from State-of-the-Art Density Functional Theory, *J. Chem.* **2015**, 495131 (2015).

[19] F. Gäbler, M. Kirchner, W. Schnelle, U. Schwarz, M. Schmitt, H. Rosner, and R. Niewa, $(Sr_3N)E$ and $(Ba_3N)E$ (E = Sb, Bi): Synthesis, Crystal Structures, and Physical Properties, *Z. anorg. allg. Chem.* **630**, 2292 (2004).

[20] E. O. Chi, W. S. Kim, N. H. Hur and D. Jung, New Mg-based antiperovskites $PnNMg_3$ (Pn=As, Sb), *J. Solid State Commun.* **121**, 309 (2002).

[21] K. Haddadi, A. Bouhemadou, and L. Louail, Structural, elastic and electronic properties of the hexagonal antiperovskites $SbNBa_3$ and $BiNBa_3$, *Comput. Mater. Sci.* **48**, 711 (2010).

[22] M. Hichour, D. Rached, M. Rabah, S. Benalia, R. Khenata, and F. Semari, Structural and elastic properties of antiperovskites $XNBa_3$ (X=As, Sb) under pressure effect, *Physica B: Condens. Matt.* **404**, 4034 (2009).

[23] D. Rached, M. Hichour, M. Rabah, S. Benalia, H. Rached, and R. Khenata, Prediction study of the structural, elastic, electronic and optical properties of the antiperovskite $BiNBa_3$, *Solid State Commun.* **149**, 2002 (2009).

[24] P. K. Jha and S. K. Gupta, First principles lattice dynamical study of the cubic antiperovskite compounds $AsNBa_3$ and $SbNBa_3$, *Solid State Commun.* **150**, 1650 (2010).

[25] I. Ullah, G. Murtaza, R. Khenata, A. Mahmood, M. Muzzamil, N. Amin and M. Saleh, Structural and Optoelectronic Properties of X_3ZN (X=Ca, Sr, Ba; Z=As, Sb, Bi) Anti-Perovskite Compounds, *J. Elec. Mater.* **45**, 3059 (2016).

[26] K. Bidai, M. Ameri, and I. Ameri, A first-principles study on structural, thermodynamics and elastic properties of $XNBa_3$ (X=As, Sb) under pressure and temperature effect, *Optik-Int. J. Light Electron Opt.* **127**, 3250 (2016).

[27] Detailed DFT studies of the band profiles and optical properties of antiperovskites $SbNCa_3$ and $BiNCa_3$, M. Bilal, I. Ahmad, H.A. R. Aliabad, and S. J. Asadabadi, *Comput. Mater. Sci.* **85**, 310 (2014).

[28] K. Haddadi, A. Bouhemadou, L. Louail, F. Rahal, and S. Maabed Prediction study of the structural, elastic and electronic properties of $ANSr_3$ (A=As, Sb and Bi), *Comput. Mater. Sci.* **46**, 881 (2009).

[29] M. Hichour, R. Khenata, D. Rached, M. Hachemaoui, A. Bouhemadou, A. H. Reshak, and F. Semari, FP-APW+lo study of the elastic, electronic and optical properties for the cubic antiperovskite $ANSr_3$ (A=As, Sb and Bi) under pressure effect, *Physica B: Condens. Matt.* **405**, 1894 (2010).

[30] M. Moakafi, R. Khenata, A. Bouhemadou, F. Semari, A. H. Reshak, and M. Rabah, Elastic, electronic and optical properties of cubic antiperovskites $SbNCa_3$ and $BiNCa_3$, *Comput. Mater. Sci.* **46**, 1051 (2009).

[31] K. Haddadi, A. Bouhemadou, L. Louail, S. Maabed, and D. Maouche, Structural and elastic properties under pressure effect of the cubic antiperovskite compounds $ANCa_3$ (A=P, As, Sb, and Bi), *Phys. Lett. A* **373**, 1777 (2009).

[32] L. Fu and C.L. Kane, Topological insulators with inversion symmetry, *Phys. Rev. B* **76**, 045302 (2007).

[33] H. Jin, S.H. Rhim, J. Im, and A.J. Freeman, Topological oxide insulator in cubic perovskite structure, *Sci. Rep.* **3**, 1651 (2013).

[34] Y. Ando, Topological insulator materials, *J. Phys. Soc. Jpn.* **82**, 102001 (2013).